Environmental Science and Pollution Research (2023) 30:111008–111020
https://doi.org/10.1007/s11356-023-30189-1

RESEARCH ARTICLE

Effective removal of Cr (VI) from aqueous solution by reinforced sodium alginate/polyethyleneimine/graphene oxide composite aerogels

Bo Gao[1] · Fei Wei[2,3] · Hongwei Yang[4] · Ji Li[2,3]

Received: 27 May 2023 / Accepted: 26 September 2023 / Published online: 6 October 2023

Abstract

A reinforced composite aerogel absorbent was synthesized using a green chemistry method and an environmentally friendly freeze-drying technique. The absorbent consisted of sodium alginate, polyethyleneimine (PEI), and graphene oxide (GO). The ability of the absorbent to remove Cr (VI) ions from aqueous solutions was studied. PEI was a nitrogen source for Cr (VI) removal and a cross-linking agent for GO sheets, while SA was a reinforcing material. The aerogel was investigated using X-ray diffraction, scanning electron microscopy, Fourier transform infrared (FTIR) spectroscopy, texture analysis, Raman spectroscopy, and thermogravimetric analysis (TGA). Batch studies were conducted to investigate the effect of pH and contact time on adsorption. The results indicated that the SA/PEI/GO aerogel had a maximum adsorption capacity of 174.05 $mg{\cdot}g^{-1}$ for Cr (VI) at pH 2. The adsorption mechanism was described using the Langmuir isotherm and pseudo-second-order kinetic models. Thermodynamic studies revealed that the adsorption process was spontaneous and endothermic. The aerogel demonstrated good regeneration ability and satisfactory recovery for Cr (VI) even after five cycles. These findings suggest that the composite aerogel could be a promising adsorbent for efficiently removing Cr (VI) from wastewater.

Keywords Graphene · Aerogel · Amination · Cr(VI) · Adsorption

Environmental Implication: Hexavalent chromium (Cr (VI)) is a pollutant that not only harms the ecological environment of water but also poses a potential threat to aquatic organisms and human health through the food chain. This issue has gained global attention, and it is urgent to find effective methods to remove Cr (VI) from water. This project has successfully developed a graphene aerogel that can efficiently remove hexavalent chromium from water. This innovation is significant in improving the water environment.

Responsible Editor: Angeles Blanco

✉ Ji Li
liji@sust.edu.cn

[1] Xi'an Key Laboratory of Advanced Photo-electronics Materials and Energy Conversion Device, School of Electronic Information, Xijing University, Xi'an 710123, People's Republic of China

[2] Key Laboratory of Auxiliary Chemistry and Technology for Chemical Industry, Ministry of Education, Shaanxi University of Science and Technology, Xi'an 710021, China

[3] Shaanxi Collaborative Innovation Center of Industrial Auxiliary Chemistry and Technology, Shaanxi University of Science and Technology, Xi'an 710021, China

[4] School of Computer Science, Xijing University, Xi'an 710123, People's Republic of China

Introduction

Water pollution by hexavalent chromium, Cr (VI), is a significant environmental concern due to its toxic and carcinogenic properties (Saha et al. 2011). Chromium is a naturally occurring element that can exist in various oxidation states, with Cr (VI) being one of the most toxic forms. This form of chromium can enter water bodies through both natural and anthropogenic sources (Hsu et al. 2010; Hashim et al. 2011). Meeting strict regulatory limits for Cr (VI) in effluent water can be challenging for some treatment methods, as they may not consistently achieve low enough concentrations.

Ion exchange resins can effectively remove Cr (VI) ions from water by exchanging them with less toxic ions. However, resin regeneration can be costly and may generate hazardous waste. The capacity of ion exchange resins can also be limited by the presence of other competing ions in the water (Li et al. 2017; Saslow et al. 2017). Chemical precipitation methods rely on the addition of reducing coagulants to convert Cr (VI) into less soluble forms, like Cr (III) or chromium hydroxide (Zhao et al. 2017). The efficiency of these methods can be hindered by the presence of interfering

substances, and the generated sludge can pose disposal challenges. Membrane-based methods like reverse osmosis and nanofiltration can effectively remove Cr (VI) from water. However, they can be expensive to install and operate, and fouling of membranes can occur, reducing their efficiency over time (Gherasim and Bourceanu 2013). Electrochemical techniques, such as electrocoagulation and electroreduction, remove Cr (VI) but may require significant energy input, and the generation of chemical byproducts can be a concern (Pan et al. 2016, 2017). Cr (VI) adsorption can be effective but adsorbents may also adsorb other ions, reducing their selectivity and efficiency. Additionally, the adsorption capacity may decrease over time, requiring frequent regeneration or replacement of adsorbents (Ge and Ma 2015; Samuel et al. 2018). Among them, adsorption is an effective, economical, and environmentally friendly technique for heavy metal treatment.

Activated carbon, chitosan, cellulose and functionalized cellulose, modified montmorillonite, MnO_2, sodium alginate (SA), polyethyleneimine (PEI), and biosorption (Alvarez et al. 2011; Liu and Huang 2011; Pang et al. 2011; Karthik and Meenakshi 2015; Gheju et al. 2016; Liu and Jin 2017; Ojembarrena et al. 2022; de Borja et al. 2022) are some of the commonly used adsorbents. It is of significant importance to highlight that over the recent years, cost-effective materials such as SA and PEI have gained substantial traction in the realm of Cr (VI) removal research. In this context, SA has demonstrated remarkable efficacy in wastewater treatment, finding successful applications through its adept processing capabilities and synergistic combinations with biochar, polyaniline, TEPA, hydroxyapatite, and chitosan (Karthik and Meenakshi 2015; Sharma et al. 2017; Periyasamy et al. 2018; Omer et al. 2019; Shakya and Agarwal 2019). Research outcomes indicate that the maximum adsorption capacity of SA-based Cr (VI) adsorbents remains relatively modest (typically below 100 mg/g). However, both SA and Ca^{2+} have garnered substantial attention as stable substrates among researchers. On the other hand, the structure of PEI chain encompasses a plethora of protonatable amino groups, thereby exhibiting exceptional Cr (VI) removal performance under acidic conditions (achieving adsorption capacities surpassing 150 mg/g for Cr (VI)). As a result, it has garnered widespread acclaim as a superlative adsorbent material for Cr (VI) mitigation. It is noteworthy, however, that PEI's excellent water solubility renders it reliant on amalgamation with other materials. Furthermore, while direct integration with certain polymers or inorganic carriers presents an avenue for hybridization, it is essential to acknowledge the drawback of potential performance degradation associated with PEI during operational usage.

GO stands as an exceptional substrate owing to its expansive specific surface area, encompassing an array of distinct functional groups including carboxyl, hydroxyl, and epoxy moieties. Moreover, GO can undergo hydrothermal reduction, leading to the formation of porous three-dimensional bulk structures characterized by an exceptionally elevated specific surface area. These characteristics underscore its efficacy in capturing heavy metal ions including Pb (II), Cd (II), Cu (II), and Hg (II) (Zhang et al. 2014; Li et al. 2015). Nevertheless, relying solely on GO for Cr (VI) removal presents inefficacies due to limitations arising from functional groups and tendencies towards aggregation. Consequently, researchers have sought to enhance the capabilities of GO for heavy metal ion adsorption through modification. For instance, Hui-Ling Ma (Ma et al. 2012) fabricated ethylenediamine-reduced GO (ED-rGO) for chemical reduction and subsequent removal of Cr (VI) from acidic aqueous solutions. Their investigation revealed that ED-rGO efficiently reduced Cr (VI) to less toxic Cr (III) at low pH levels. In a similar vein, Xiaoshu Lv (Lv et al. 2014) synthesized nanoscale zero-valent iron (nZVI) incorporated onto magnetic Fe_3O_4/graphene (nZVI@MG) nanocomposites to extract Cr (VI) from aqueous solutions. Experimental findings demonstrated a Cr (VI) removal efficiency of 83.8%, significantly surpassing the performances of individual components (nZVI, Fe_3O_4 NPs, and graphene). To summarize, the amalgamation of GO and PEI takes place under mild conditions, facilitated by amino and epoxy groups. This process results in a composite with calcium alginate, engendering an interpenetrating network architecture. Consequently, the material acquires a combination of elevated specific surface area and abundant Cr (VI) adsorption capability, attributed to the effective interaction of functional groups. Notably, this composite exhibits substantial stability, rendering it a proficient adsorbent for Cr (VI) removal.

This study uses sodium alginate as a reinforcing material to develop a highly porous and interconnected GO aerogel with enhanced strength. The resulting material, sodium alginate/polyethylenimine/graphene oxide aerogel (SA/PEI/GO), was an efficient adsorbent for removing Cr (VI) from aqueous solutions. As a nitrogen source and cross-linking agent, PEI provided additional adsorption sites for removing Cr (VI). Using SA/PEI/GO as an adsorbent demonstrates a novel and effective approach to improving the adsorption performance in treating Cr (VI) contaminated wastewater.

Experimental

Materials and reagents

Graphite powders were purchased at Qingdao Heilong Graphite Co.Ltd(Qingdao, China). Ethylene imine polymer (PEI, M_w=10000 g/mol, 99%). Phosphorus pentoxide (P_2O_5) was acquired from Shanghai Mecklin Biochemical Co.Ltd. Sodium alginate (SA, M=250000g/mol) was purchased

from Tianjin Fuchen Chemical Reagents Co., Ltd. (Tianjin, China). Concentrated sulfuric acid (H_2SO_4 98.8%) was obtained from Luoyang Haohua Chemical Reagents Co., Ltd. (Luoyang, China). Sodium nitrate ($NaNO_3$), anhydrous calcium chloride ($CaCl_2$), potassium persulfate ($K_2S_2O_8$), and potassium permanganate ($KMnO_4$) are provided by Tianjin Chemical Reagent Co., Ltd. Ethanol was from Tianjin Fuyu Fine Chemical Co., Ltd. All chemicals were used without further purification.

Preparation of GO

The GO preparation involved natural graphite powders and a modified Hummers method (Hummers and Offeman 1958; Marcano et al. 2010). The resulting GO was then dispersed in deionized water using a gentle ultrasonic treatment for over 1 h. The pH of the GO dispersion was adjusted to 8.0 by adding drops of 0.1 M aqueous sodium hydroxide solution until the desired pH was reached.

Preparation of SA/PEI/GO

To synthesize the SA/PEI/GO hybrid aerogel, 120 mg of SA was dissolved in 3 mL of deionized water and stirred for 1 h to obtain a transparent SA solution. Then, 40 mg of PEI was added, stirring the mixture until uniform. Next, the GO dispersion (8 mg·mL^{-1}) was added and stirred for 10 min to prepare a hybrid sol. The precursor was then stored at 60°C for 24 h to form a hydrogel immersed in a 2 wt% $CaCl_2$ aqueous solution for over 12 h to achieve an interpenetrating network structure. The bulk was dialyzed with deionized water to remove excess $CaCl_2$, SA, and unattached PEI. Finally, the hydrogel was frozen at −50°C and freeze-dried under a vacuum (less than 10 Pa) for 48 h to obtain the SA/PEI/GO aerogel.

Adsorption behavior of SA/PEI/GO for Cr(VI)

Adsorption experiments were conducted in a temperature-controlled water batch shaker (SHZ-82) at 313 K using a 30-mL glass flask containing the solution with the desired pH and contact time. After achieving adsorption equilibrium, the remaining concentration of Cr (VI) was determined using a UV-Vis spectrophotometer (Evolution 220, Thermo Fisher Scientific, America) at a wavelength of 544 nm (the quantitative method for Cr (VI) can be found in the experimental section in the electronic supplementary information and Supplementary Figure 1). The adsorption capacity and removal efficiency were calculated using Eqs. (1) and (2):

$$q_e = \left(\frac{C_0 - C_e}{m}\right)v \tag{1}$$

$$\eta = \frac{\left(C_0 - C_e\right)}{c_0} \times 100\% \tag{2}$$

where C_0 (mg·L^{-1}) and C_e (mg·L^{-1}) are the Cr (VI) concentrations at initial and at equilibrium, respectively. V is the volume of the solution (mL) and m is the mass of SA/PEI/GO aerogel (mg).

Characterization

The transmission electron microscope (TEM, Tecnai G2 F20 S-TWIN, America) was used to analyze the morphology of GO. The scanning electron microscope (SEM, Verios 460, FEI, America) was used to observe the morphology of the SA/PEI/GO aerogel. The texture analyzer (TMS-PRO, FTC, America) was used to test the mechanical properties. Fourier transform infrared spectroscopy (FT-IR) spectrum was recorded using FT-IR spectroscopy (Vertex70, Burker, Germany). X-ray diffraction (XRD) experiments were conducted on specimens from 4° to 60° using an X-ray diffractometer (D8 Advance, Bruker, Germany). Thermogravimetric analysis (TGA) tests were carried out from 298 to 973 K at a rate of 10 K/min in an argon environment using the TG/DTA thermogravimetric analyzer (STA449F3-1052-M, Netsal, Germany). The Thermo Scientific DXR high-resolution Raman microscope (THEM, America) was used for Raman measurement. The surface functionalities and elemental composition of SA/PEI/GO aerogel were analyzed using an X-ray photoelectron spectroscopy (XPS, AXIS SUPRA, America).

Results and discussion

Mechanical properties of aerogels

The SA/PEI/GO hydrogel prepared in this study removes Cr (VI) from aqueous solutions. The mechanical properties of adsorbent materials are crucial for their applicability and recyclability. SA was employed as a reinforcing agent to enhance the mechanical properties of the GO-based aerogel. Therefore, the texture analyzer was employed to evaluate the mechanical properties of composite hydrogels, and the findings are presented in Table 1. The desired improvement in the hardness of composite hydrogel was made by adding SA.

In contrast, the springiness and resilience of hydrogels marginally decreased with increasing SA dosage due to the high rigidity of SA in the gel system. GO, being a flexible material, contributes to the flexibility of the composite. As a

Table 1 The mechanical properties of hydrogels were evaluated by preparing samples with varying concentrations of SA

Concentration of SA (mg mL^{-1})	Hardness	Springiness	Cohesiveness	Resilience
20	56.072	0.804	0.421	0.182
30	127.619	0.727	0.579	0.156
40	292.283	0.685	0.651	0.123
50	441.035	0.676	0.714	0.106

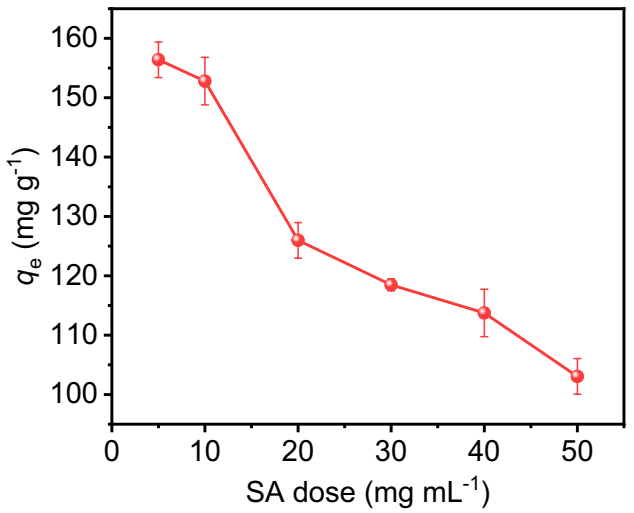

Fig. 1 Effect of SA concentration on Cr (VI) adsorption capacity of SA/PEI/GO materials

result, the combination of GO's flexibility and SA's rigidity increases the composite hydrogel's strength and flexibility.

The presence of SA significantly impacted the adsorption properties of SA/PEI/GO. As shown in Fig. 1, the adsorption capacity of SA/PEI/GO for Cr (VI) dropped rapidly as the SA dosage increased. It is due to SA considerably reducing the specific surface area of aerogels and occupying some active adsorption sites in the composite aerogels. Therefore, to achieve a composite aerogel with both high strength and excellent adsorption properties, the optimum concentration of SA was determined to be 30 mg·mL^{-1}, which was used in subsequent experiments.

Microstructures and morphologies of GO and SA/PEI/GO

Figure 2a depicts the morphology of the GO we prepared, displaying the typical characteristics of a two-dimensional material. It has larger dimensions in the horizontal direction and smaller sizes with wrinkled edges in the thickness direction, indicating the successful oxidation and exfoliation of graphite. By incorporating PEI and SA and undergoing thermal reduction, the original GO solution transformed into a three-dimensional state, as shown in Fig. 2b. Our SA/PEI/GO material exhibits a distinct difference in morphology from GO. SA/PEI/GO displays an unordered stacking structure of multiple layers (two-dimensional material structure), which arises due to the π-π stacking of GO layers during the thermal reduction process. The loose structure ensures rapid mass transfer and guarantees low density, which is advantageous for aerogels used as adsorbents. Additionally, the thickness of the pore walls in SA/PEI/GO reaches approximately 2 μm (illustrated in inset of Fig. 2b and c), indicating a significant increase compared to the thickness of GO. This increase results from both the stacking of GO and the introduction of sodium alginate and PEI chains. At higher magnification, the SEM images (Fig. 2d) reveal that the pore walls consist of an open pore structure with multiple levels. This arrangement is probably a result of hydrophilic polymer aggregation as the material dries. This characteristic not only reinforces the mechanical integrity of the aerogel but also offers a more extensive surface area, beneficial for the adsorption of Cr (VI).

Structure analysis of SA/PEI/GO

The characterization and confirmation of SA/PEI/GO formation were carried out using various techniques, including FT-IR, XRD, Raman, XPS, and TGA. Figure 3 depicts the FT-IR spectra of GO, GA, and SA/PEI/GO. The presence of several characteristic peaks in the GO spectrum indicates the successful preparation of the material. Specifically, the broad peak observed at 3369 cm^{-1} corresponds to the stretching vibration of the O-H group. The peak at 1732 cm^{-1} corresponds to the stretching vibration of the C=O bond in the carboxyl group. The C=C stretching vibration on the aromatic ring is responsible for the peak at 1625 cm^{-1}, whereas the COH bending vibration is responsible for 1385 cm^{-1}. Finally, the signal at 1081 cm^{-1} is assigned to the epoxy group's COC (Ge and Ma 2015). Upon comparing with GO, two new peaks appeared at 2942 cm^{-1} and 2837 cm^{-1} in SA/PEI/GO, assignable to the symmetric and asymmetric stretching modes of $-CH_2-$ of the PEI chains. Additionally, distinct peaks at 1595 cm^{-1} and 1430 cm^{-1} in SA/PEI/GO were attributed to C−N-stretching and N-H-bending vibrations, indicating that the successful cross-linking and functionalization of GO by PEI (Sui et al. 2013). In comparison to the infrared spectrum of SA, the carboxylate group at 1649 cm^{-1} in our SA/PEI/GO composite exhibited a notable redshift. This phenomenon can be attributed to the alteration in the charge density, radius, and atomic mass of the cation upon the substitution of sodium ions with calcium metal ions in sodium alginate (Daemi and Barikani 2012). The observed peak partially coincided with the CO-NH

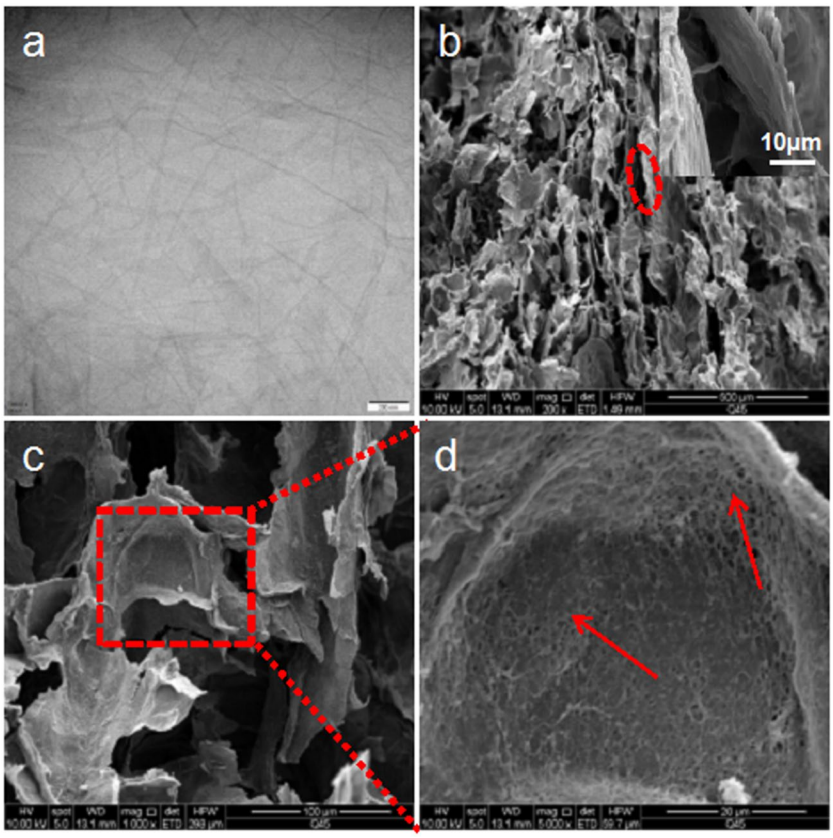

Fig. 2 **a** TEM image of GO, **b**, **c**, **d** SEM images of SA/PEI/GO in different magnification

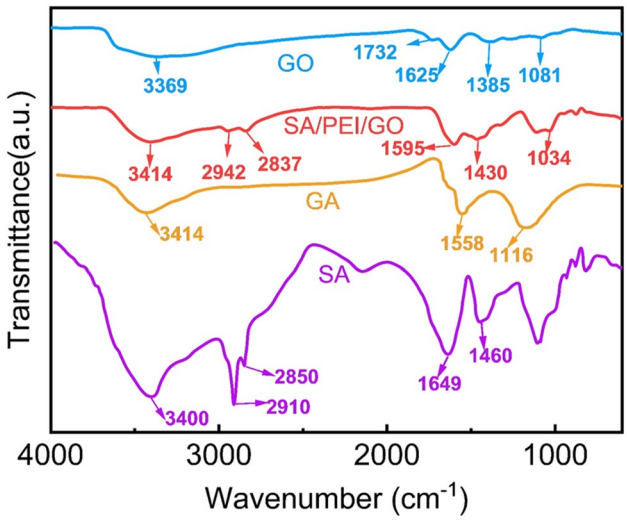

Fig. 3 FT-IR spectra of GO, GA, and SA/PEI/GO

vibration. Hence, the schematic representation of the structure of our SA/PEI/GO composite is depicted in Scheme 1.

The crystal structure and interlayer spacing of samples were analyzed using XRD. Figure 4 shows the XRD pattern of GN, GO, and SA/PEI/GO. GN shows an obvious diffraction peak at 26.43° corresponding to the (002) crystal plane, indicating high crystallinity with an interlayer spacing of 0.34 nm. The typical diffraction peak at 10.32° of GO suggests an expanded interlayer spacing of 0.86 nm due to the abundant O-containing functional groups on its surfaces created by the modified Hummers method (Yang et al. 2014; Cao et al. 2017). However, SA/PEI/GO has no clear peak, and its crystallinity drops dramatically. It is due to the covalent and non-covalent interactions between PEI chains and GO sheets and the interpenetrating network structure generated by SA in the 3D structure. If GO is cross-linked on the edges or sides of the sheet and its regular stacks are disrupted, the diffraction peaks in the XRD pattern become weak or even disappear (Cai and Song 2007; Xu et al. 2008).

We used Raman spectroscopy to further investigate the chemical structures of GN, GO, and SA/PEI/GO (see Fig. 5). Due to the presence of a layered structure consisting of entirely sp^2 hybridized forms of carbon atoms in the graphite, GN exhibits only a G band of 1548 cm^{-1} (Ferrari and Robertson 2000). On the other hand, GO exhibited two characteristic bands, the D band (1349 cm^{-1}) and the G band (1579 cm^{-1}), which are associated with the sp^2-hybridized carbon structure and the defect structure induced by hydroxyl or epoxide groups, respectively (Ferrari et al. 2006). The I_D/I_G ratio of GO was 0.91. In contrast, for SA/PEI/GO, the D and G bands were observed at 1351 cm^{-1} and 1596 cm^{-1},

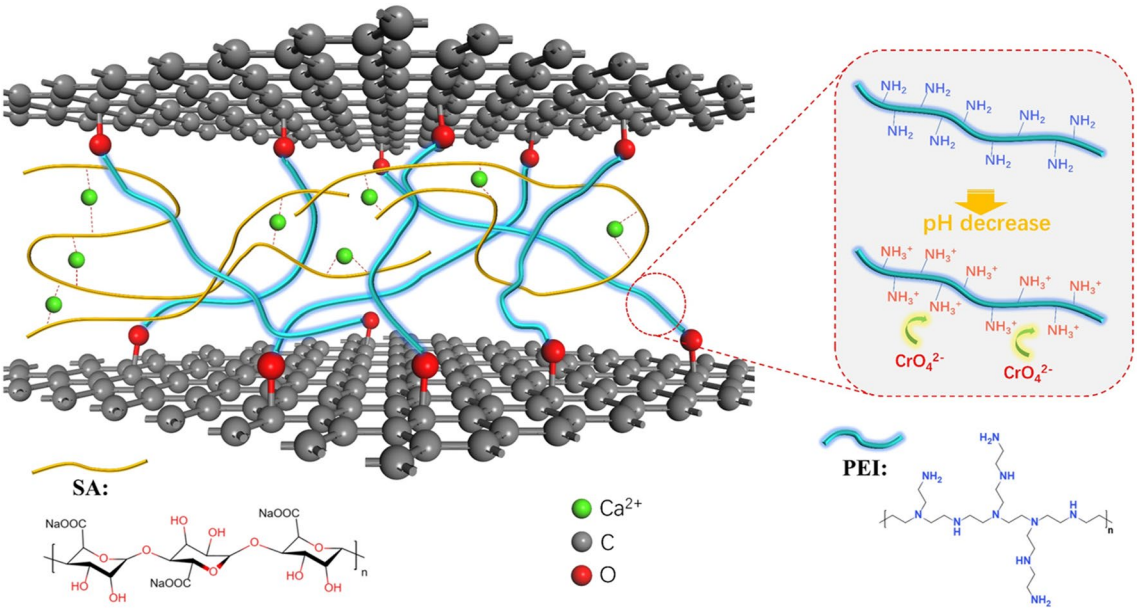

Scheme 1 The structure of SA/PEI/GO and the schematic diagram illustrating the mechanism of Cr (VI) adsorption

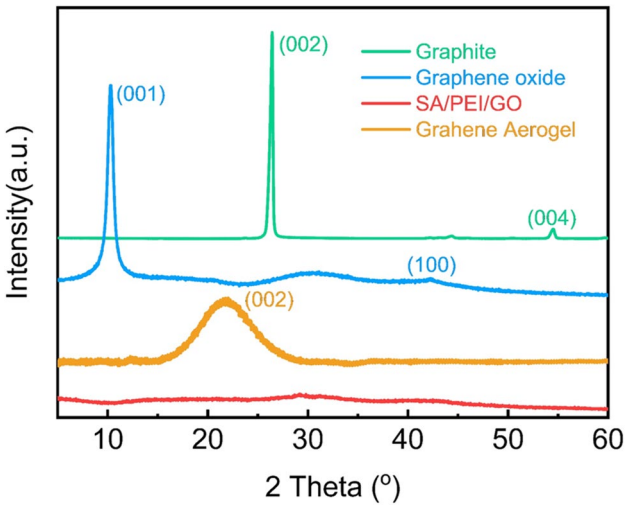

Fig. 4 XRD pattern of graphite, GO, GA, and SA/PEI/GO

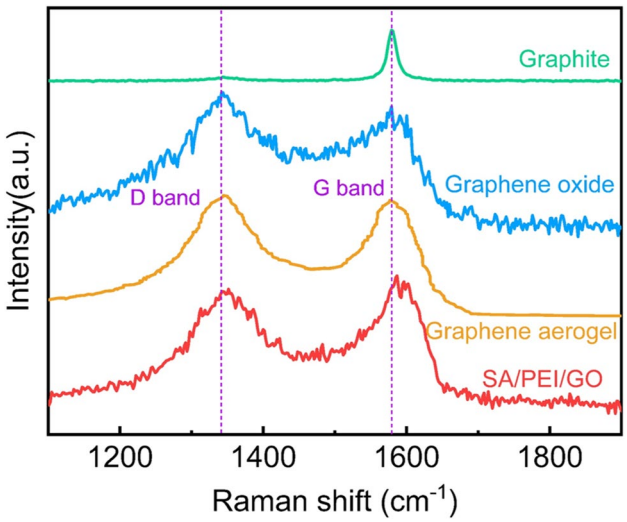

Fig. 5 Raman spectra of GN, GO, GA, and SA/PEI/GO

respectively. The I_D/I_G ratio of SA/PEI/GO was around 1.16, which was higher than that of GO, indicating that introducing N atoms of PEI and the molecular chains of SA onto the carbon framework caused the defects (Yang et al. 2018).

XPS was used for GO and SA/PEI/GO surface analysis. Figure 6a shows the full spectra of GO and SA/PEI/GO. GO exhibits two peaks at 284 eV and 532 eV attributed to C1s and O1s, respectively. SA/PEI/GO produces two new peaks, N1 and Ca2p, at 398 and 346 eV, respectively, indicating that PEI chains have been successfully introduced into graphene aerogels. The high-resolution C1s spectra of GO in Fig. 6b exhibit four peaks at 284.6 eV, 285.2 eV, 286.8 eV, and 288.5 eV, attributed to C-C/C=C, C-OH, C-O-C, and C=O, respectively. Compared with GO, the C1s spectrum of SA/PEI/GO peaks at 285.3 eV, indicating C-N and C-OH functional groups. The N1s spectrum of SA/PEI/GO reveals three peaks at 398.6 eV, 399.4 eV, and 401.0 eV, corresponding to NH(R), N-C=O, and $-NH_2$, respectively. These findings suggest that the amino group on PEI chains reacted

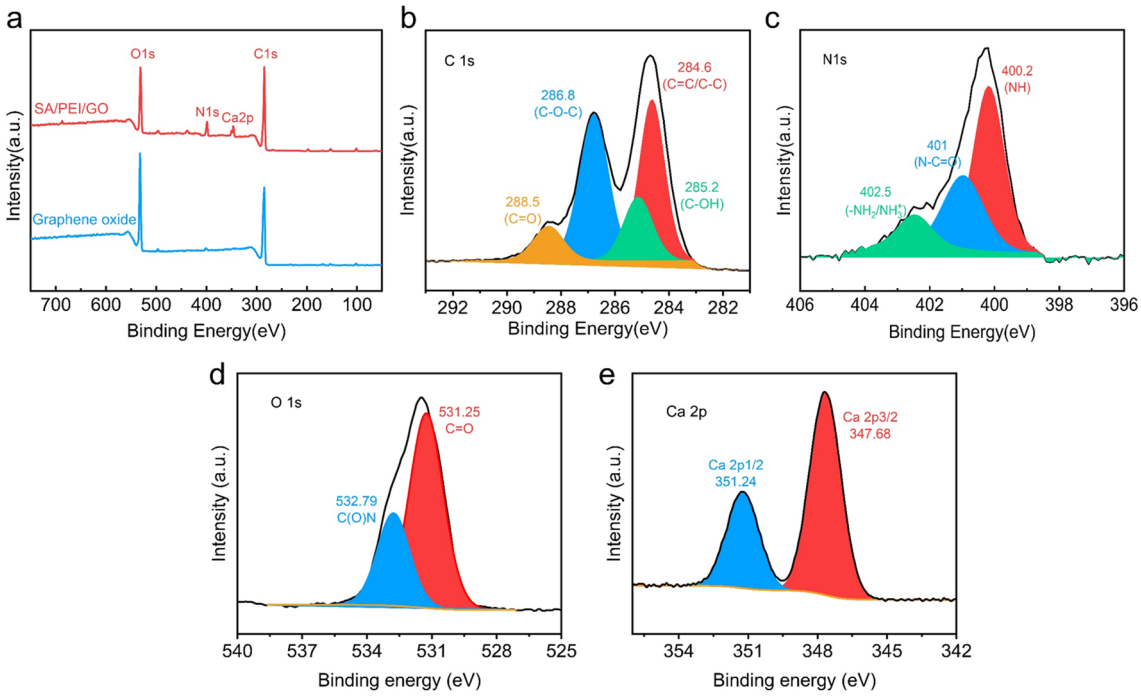

Fig. 6 Full range XPS spectra of GO and SA/PEI/GO (**a**), C1s XPS spectra of GO (**b**), N1s XPS spectra of SA/PEI/GO (**c**), O1s XPS spectra of SA/PEI/GO (**d**), and Ca2p XPS spectra of SA/PEI/GO (**e**)

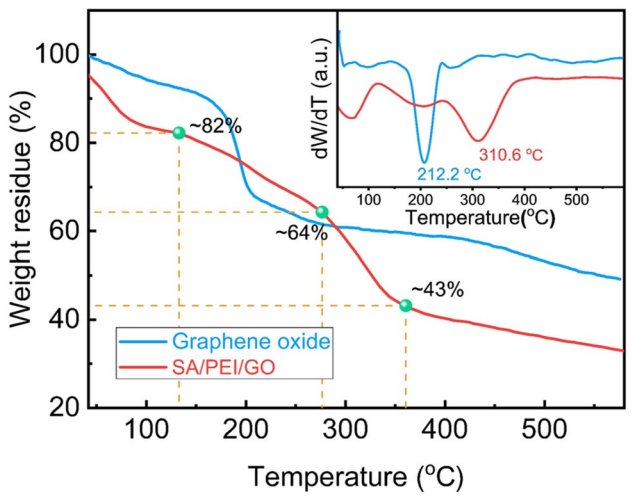

Fig. 7 The TGA curves of GO and SA/PEI/GO

with the oxygen-containing functional groups on GO layers, consistent with the FT-IR analysis.

Thermogravimetric analysis was used to investigate the composition of our SA/PEI/GO, and the results are shown in Fig. 7. The TG curve of GO shows a significant weight loss at about 212.2°C due to the thermal decomposition of the oxygen-containing functional groups on the surface. On the other hand, SA/PEI/GO displays three distinct stages of thermal degradation: the first stage involves the removal of adsorbed water on SA/PEI/GO at around 71.6°C, the second stage corresponds to the decomposition of PEI at about 206.2°C (Sui et al. 2013), and the third stage corresponds to the decomposition of SA at around 310.6°C (Jiao et al. 2016). The findings indicate that the synthesized adsorbent is indeed composed of SA, PEI, and GA, with mass percentages of 21%, 18%, and 43%, respectively.

Effect of initial pH for Cr(VI) adsorption

In the process of adsorption of Cr (VI) by SA/PEI/GO as adsorbent, the initial pH of the solution is a significant controlling factor. Generally, the existence of Cr (VI) depends on the pH of the solution (Saha and Orvig 2010). When the solution pH is below 2, the major Cr (VI) forms are $HCrO_4^-$ and H_2CrO_4. At pH of 2–6, Cr (VI) exists mainly in $HCrO_4^-$. The major ion form of Cr (VI) is CrO_4^{2-} above pH 6. As shown in Fig. 8, the effect of initial pH was studied in the range of 1–11, where adsorption capacity reached a maximum value of

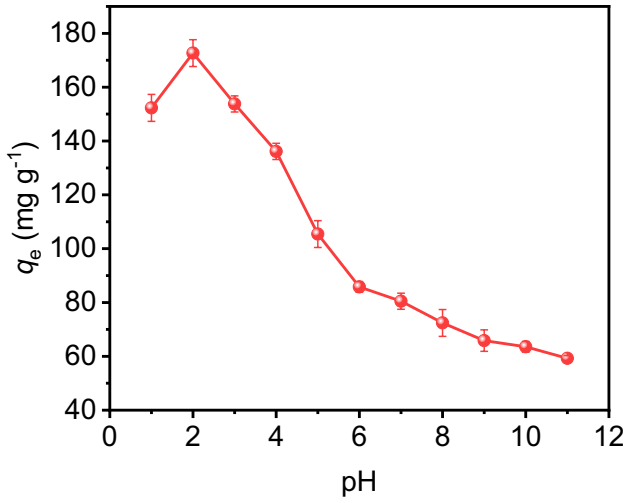

Fig. 8 The effect of pH on Cr (VI) adsorption performance by SA/PEI/GO

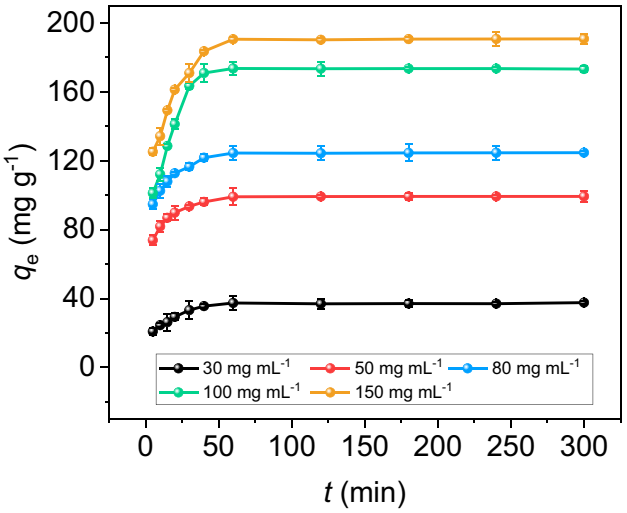

Fig. 9 The effect of contact time on Cr (VI) by SA/PEI/GO

174.05 mg g^{-1} at pH 2 (Chauke et al. 2015). This adsorption capacity was comparably higher compared to other adsorbent materials, as indicated in the supplementary Table S1. In other studies, the maximum removal of Cr (VI) is at pH 3 as when using nanocellulose (Ojembarrena et al. 2022; de Borja Ojembarrena et al. 2022). It can be explained by examining the surface charge of the SA/PEI/GO adsorbent (the results can be found in Figure S2 of the supplementary information). By means of zeta potential analysis, it was ascertained that the isoelectric point of our SA/PEI/GO adsorbent is approximately 8.6. At lower pH, the amino groups of the SA/PEI/GO could be protonated to form positively charged sites($-NH_3^+$), which resulted in the strong electrostatic interaction with the anionic Cr (VI). Meanwhile, it is indicated that the SA/PEI/GO prefer to adsorb $HCrO_4^-$ rather than $Cr_2O_7^{2-}$ and CrO_4^{2-}. The reason is that compared with $Cr_2O_7^{2-}$ and CrO_4^{2-}, $HCrO_4^-$ has a smaller size (Hozhabr Araghi et al. 2015), accelerating the intraparticle diffusion of $HCrO_4^-$ and making it combine with the positive charge on the adsorbent surface efficiently and quickly, and the adsorption capacity reaches the maximum. With the increase of pH, the positive charge on the surface of SA/PEI/GO decreases sharply due to deprotonation, resulting in the decrease of adsorption; in addition, there is competition between OH^- and Cr (VI) anions in alkaline media for adsorption, which also decreases the adsorption amount.

The role of initial solution pH in the adsorption of Cr (VI) by SA/PEI/GO adsorbent was investigated and found to be a significant factor (Saha and Orvig 2010). The speciation of Cr (VI) depends on solution pH, with $HCrO_4^-$ and H_2CrO_4 being the dominant species at pH below 2 and CrO_4^{2-} the major ion form above pH 6. The effect of initial pH on adsorption capacity was studied in the pH range of 1–11, and it was observed that the maximum adsorption capacity was achieved at pH 2 (see Fig. 8) (Chauke et al. 2015). This phenomenon can be explained by the surface charge of the SA/PEI/GO adsorbent. At lower pH, protonation of amino groups on SA/PEI/GO leads to the formation of positively charged sites ($-NH_3^+$), which facilitates strong electrostatic interaction with anionic Cr (VI). The preference of SA/PEI/GO for $HCrO_4^-$ over $Cr_2O_7^{2-}$ and CrO_4^{2-} can be attributed to the smaller size of $HCrO_4^-$ which enables faster intraparticle diffusion and efficient combination with positive charges on the adsorbent surface. As pH increases, the positive charge on the SA/PEI/GO surface decreases due to deprotonation, reducing adsorption. Additionally, the increase of OH^- in alkaline media competes with Cr (VI) anion and occupies some adsorption sites, resulting in a continuous decrease in adsorption efficiency.

Effect of contact time for Cr(VI) adsorption

The influence of contact time on removing Cr (VI) by SA/PEI/GO was investigated. The findings are presented in Fig. 9. During the initial stage of adsorption (the first 30 min), the adsorption capacity increased rapidly, which can be attributed to the high number of active adsorption

sites on the SA/PEI/GO adsorbent surface. However, as the contact time increased, the available adsorption sites decreased, leading to a slower rise in adsorption capacity. In addition, the repulsive forces between Cr (VI) and the adsorbent surface phase (Zhang et al. 2016) lead to a reduced driving force and, therefore, a slower diffusion rate (Kong et al. 2014). After 60 min, the adsorption capacity of SA/PEI/GO reached an equilibrium state, indicating that all adsorption sites were fully occupied. Therefore, based on these results, a contact time of 60 min was selected as the optimal duration for subsequent experiments.

Adsorption kinetics

The kinetic study mainly determines the adsorption mechanism, including chemical reaction, physical reaction, diffusion control and mass transfer (Moussavi and Khosravi 2010). It can also provide valuable insight into the adsorption pathways and reaction process (Vilcinskas et al. 2016). Therefore, to characterize the kinetics of Cr (VI) adsorption on SA/PEI/GO, the experimental adsorption data were analyzed kinetically using the commonly used quasi-primary and quasi-secondary kinetic models. The adsorbent's performance was investigated for different initial concentrations of Cr (VI) (30, 50, 80, 100, and 150 mg L^{-1}). The pseudo-first-order model and the pseudo-second-order model are expressed as follows:

The purpose of sorption kinetic studies is to determine the adsorption mechanism, including chemical and physical reactions, diffusion control, and mass transfer (Moussavi and Khosravi 2010). These studies can also provide valuable insight into adsorption pathways and reaction processes (Vilcinskas et al. 2016). To investigate the dynamic characteristics of Cr (VI) adsorption on SA/PEI/GO, the commonly used pseudo-first-order and pseudo-second-order kinetic models were applied to the experimental data obtained from different initial Cr (VI) concentrations (30, 50, 80, 100, and 150 mg·L^{-1}). The pseudo-first-order and pseudo-second-order models are expressed as follows:

$$\log\left(q_e - q_t\right) = \log q_e - \frac{k_1 t}{2.303} \tag{3}$$

$$\frac{t}{q_t} = \frac{t}{q_e} + \frac{1}{k_2 q_e^2} \tag{4}$$

where q_e is the equilibrium adsorption capacity of Cr (VI) (mg g^{-1}), q_t (mg g^{-1}) is the adsorption capacity of Cr (VI) at time t (min), and k_1 (min^{-1}) and k_2 (g mg^{-1} min^{-1}) are the rate constants of the pseudo-first-order and pseudo-second-order models, respectively.

Figure 10 shows the plots for pseudo-first-order and pseudo-second-order models for Cr (VI) adsorption, and the calculated kinetic parameters are presented in Table 2. The results indicate that the pseudo-second-order kinetic model can better fit the experimental data with higher

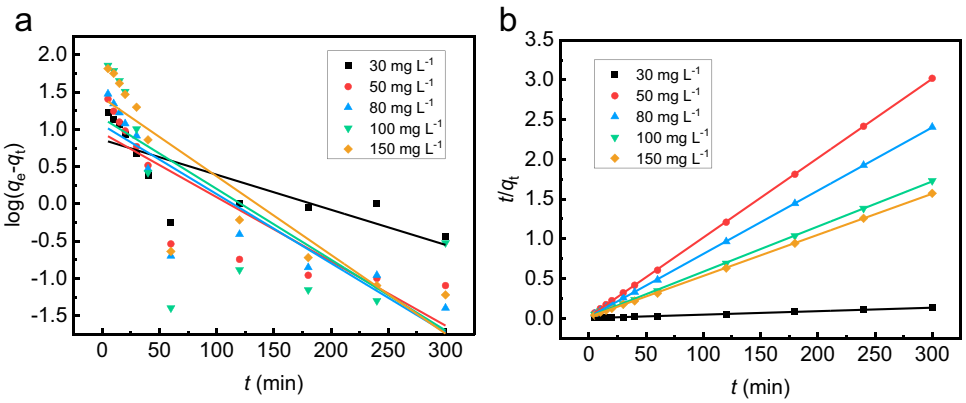

Fig. 10 The kinetic studies for the adsorption of Cr (VI) by SA/PEI/GO: **a** plot for the first-order model, **b** plot for second-order model

Table 2 Kinetic parameters for the adsorption of SA/PEI/GO on Cr(VI)

C_0 (mg·L^{-1})	Pseudo-first-order			Pseudo-first-order		
	K_1 (min^{-1})	$Q_{e,cal}$ (mg·g^{-1})	R^2	K_2 (g/(mg·min))	$Q_{e,cal}$ (mg·g^{-1})	R^2
30	2.04×10^{-3}	7.29743	0.603	3.72×10^{-1}	37.21609	0.999
50	3.74×10^{-3}	8.95694	0.747	5.66×10^{-3}	99.31324	0.999
80	4.02×10^{-3}	11.48312	0.775	4.52×10^{-3}	124.62347	0.999
100	4.12×10^{-3}	14.17881	0.481	1.72×10^{-3}	173.54921	0.999
150	4.58×10^{-3}	26.72329	0.768	1.69×10^{-3}	190.74108	0.999

correlation coefficients (R^2>0.999). Additionally, the pseudo-second-order model's calculated adsorption capacity ($Q_{e,\,cal}$) is very close to the experimental values. Therefore, it can be concluded that the adsorption of Cr (VI) on SA/PEI/GO follows the pseudo-second-order model, and the rate of the adsorption process in this study was controlled by chemisorption. These findings provide valuable insights into the adsorption pathways and reaction process of Cr (VI) on SA/PEI/GO (Ho et al. 2011; Zhou et al. 2017).

Combining the research findings on the influence of initial pH on Cr (VI) adsorption, we propose the adsorption mechanism of SA/PEI/ GO on Cr (VI) as shown in Scheme 1. At low pH values, the PEI within the adsorbent becomes protonated, creating more positively charged adsorption sites. These sites interact strongly with the negatively charged Cr (VI), aligning with the conclusions drawn from the adsorption kinetics studies. Conversely, as the pH increases, the $-NH_2$ or $-NH-$ groups within PEI undergo deprotonation, leading to a weakening of the interactions between the adsorbent and Cr (VI).

Adsorption isotherms

To gain a deeper insight into the equilibrium relationship between the amount of Cr (VI) adsorbed onto the solid surface and the amount remaining in the liquid phase, adsorption isotherms were investigated. The isotherms were generated by varying the initial Cr (VI) concentration between 20 and 260 mg L^{-1} at different temperatures (20°C, 30°C, and 40°C). The adsorption isotherm data were fitted using Langmuir and Freundlich isotherm models.

The Langmuir model assumes that adsorption occurs on a homogeneous surface of the adsorbent as a monolayer, and there is no interaction between adsorbate molecules during the adsorption process (Foo and Hameed 2010). On the other hand, the Freundlich isotherm model is used to describe heterogeneous and multilayer adsorption (Tonghuan et al. 2013). The Langmuir and Freundlich isotherm equations can be expressed as follows:

$$\frac{C_e}{q_e} = \frac{C_e}{q_m} + \frac{1}{bq_m} \tag{5}$$

$$\ln q_e = \ln K_F + \frac{1}{n} \ln C_e \tag{6}$$

where C_e is the equilibrium concentration of Cr (VI) (mg L^{-1}), q_e is the equilibrium adsorption capacity (mg g^{-1}), q_m is the maximum adsorption capacity of adsorbents, and b is Langmuir constant (L mg^{-1}). n and K_F are the Freundlich constants related to adsorption intensity and capacity, respectively.

The adsorption isotherm data were analyzed using Langmuir and Freundlich models, as shown in Fig. 11. The calculated parameters are presented in Table 3. The Langmuir model provided a better fit to the data with a higher correlation coefficient (R^2>0.99) than the Freundlich model, suggesting that the adsorption of Cr (VI) onto SA/PEI/GO was a monolayer adsorption reaction with a fixed number of binding sites

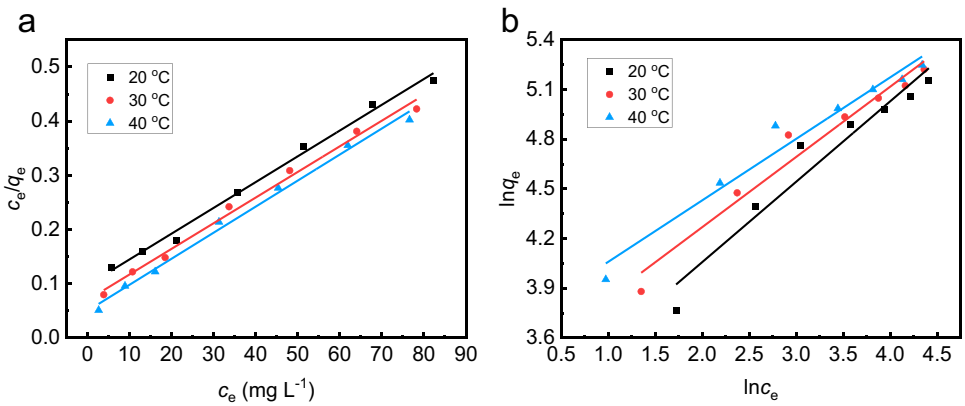

Fig. 11 Langmuir isotherm (**a**) and Freundlich isotherm (**b**) for adsorption of SA/PEI/GO on Cr (VI) at different temperature

Table 3 Langmuir and Freundlich isotherm parameter for adsorption of SA/PEI/GO on Cr(VI)

T(°C)	Langmuir			Freundlich		
	R^2	b (L mg^{-1})	q_m (mg g^{-1})	R^2	1/n	k_F
20	0.992	0.04896	210.08403	0.929	0.48587	21.89175
30	0.992	0.06786	211.41649	0.954	0.42442	30.57522
40	0.992	0.09637	207.90020	0.958	0.37159	39.95645

Table 4 Thermodynamic parameters for adsorption of Cr(VI) by SA/PEI/GO

Temperature (K)	ΔH (kJ mol^{-1})	ΔG (kJ mol^{-1})	ΔS (kJ mol^{-1}·K^{-1})
293	4.2756	−5.0135	0.031539
303	4.2756	−5.9354	0.033541
313	4.2756	−7.0031	0.035881

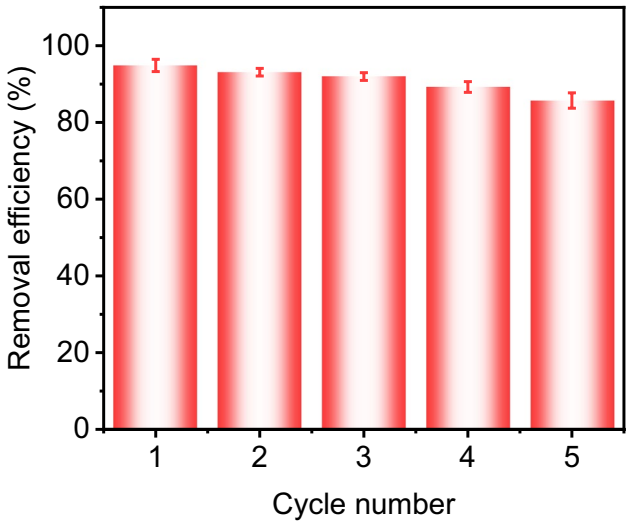

Fig. 12 Regeneration study of SA/PEI/GO

(Zhou et al. 2016). With increasing temperature, the increased *b* values of SA/PEI/GO indicated that the Cr (VI) adsorption on SA/PEI/GO was endothermic (Wang et al. 2010). Additionally, the *n* values of the Freundlich model were greater than 1 at different temperatures, indicating that the adsorption of Cr (VI) onto SA/PEI/GO was favorable. Therefore, SA/PEI/GO can be considered an excellent adsorbent.

Adsorption thermodynamics

The thermodynamic characteristics of Cr (VI) adsorption on SA/PEI/GO, including enthalpy change (ΔH), free energy change (ΔG), and entropy change (ΔS), are calculated using the following equations:

$$\ln K = -\frac{\Delta H}{RT} + \frac{\Delta S}{R} \tag{7}$$

$$\Delta G = -\ln KRT \tag{8}$$

where K is the standard thermodynamic equilibrium constant (mg L^{-1}), R is the gas constant (8.314 J mol$^{-1}K^{-1}$), and T is the absolute temperature (K).

Table 4 summarizes the thermodynamic parameters, including ΔH, ΔS, and ΔG, for the adsorption process of Cr (VI) by SA/PEI/GO. The negative values of ΔG indicated that the adsorption process was spontaneous. The positive values of ΔH indicated that the adsorption process was endothermic, consistent with the results obtained from isotherm analysis. Additionally, a positive value of ΔS indicates an increase in disorder at the solid–liquid interface during adsorption (Singh et al. 2017).

Reusability of SA/PEI/GO

The ability to regenerate the adsorbent is critical in evaluating its performance. SA/PEI/GO could remove weakly bound Cr (VI) ions using an alkaline solution as an eluent. In this study, 0.2 M NaOH was utilized to regenerate SA/PEI/GO, and the adsorption–desorption experiments were performed for five cycles to examine the reusability of the adsorbent. The results in Fig. 12 demonstrate that SA/PEI/GO has exceptional regeneration properties, with a decrease in Cr (VI) removal rate of only about 10% and retention of > 85% after five cycles. This decline in removal efficiency may be attributed to reducing some Cr (VI) to Cr (III) by hydroxyl groups on SA/PEI/GO, resulting in precipitated Cr_2O_3 that adheres to the surface or interior of SA/PEI/GO (Li et al. 2013). Moreover, the adsorption–desorption experiment employed NaOH as the eluent, a factor which could induce the dissolution of reinforcement material (i.e., calcium alginate). This phenomenon might lead to the partial disruption of the aerogel's pore architecture, consequently contributing to a reduction in the adsorption efficacy of SA/PEI/GO.

Conclusion

The SA/PEI/GO material was successfully prepared using a green chemistry method and an environmentally friendly freeze-drying technique. Characterization using FTIR, texture analyzer, SEM, XRD, XPS, Raman, and TGA techniques showed that introducing SA greatly improved hydrogels' mechanical properties. The SA/PEI/GO material exhibited a 3D network porous structure with rich amino groups, making it an effective adsorbent for Cr (VI) removal, achieving an adsorption capacity of up to 174.05 mg g^{-1} at pH 2. The adsorption process is consistent with pseudo-secondary kinetics and the Langmuir model and is spontaneous and exothermic. Moreover, the SA/PEI/GO material showed great regeneration after five cycles, making it an efficient and reusable adsorbent for Cr (VI) removal from wastewater.

Supplementary Information The online version contains supplementary material available at https://doi.org/10.1007/s11356-023-30189-1.

Author contributions Ji Li conceived the idea, designed the experiments, and wrote the manuscript. Bo Gao designed the experiments with Ji Li, prepared the materials and performed the adsorption measurements, and analyzed the results with Ji Li. Bo Gao and Ji Li analyzed the data and wrote the manuscript. Fei Wei carried out the FTIR, XRD, and XPS measurements. Hongwei Gao discussed the data with Bo Gao and performed TEM on the graphene oxide and aerogel. All the authors edited the manuscript before submission.

Funding We acknowledge the National Key R&D Program of China (2017YFB0308500) for the financial support of our research. This project was supported by The Youth Innovation Team of Shaanxi Universities (22JP006). It was supported by the Open Foundation of Key Laboratory of Auxiliary Chemistry and Technology for Chemical Industry, Ministry of Education, Shaanxi University of Science and Technology (No. KFKT2022-13) and Shaanxi Collaborative Innovation Center of Industrial Auxiliary Chemistry and Technology, Shaanxi University of Science and Technology (No. KFKT2022-13).

Data availability All data are provided in the manuscript.

Declarations

Ethics approval Ethical approval is not involved in the manuscript.

Consent to participate All authors made substantial contributions to the conception design, data interpretation, and all steps involved in this work.

Consent for publication All authors have approved the version to be published.

Conflict of interest The authors declare no competing interests.

References

Alvarez GS, Foglia ML, Camporotondi DE et al (2011) A functional material that combines the Cr(VI) reduction activity of *Burkholderia* sp. with the adsorbent capacity of sol–gel materials. J Mater Chem 21:6359–6364. https://doi.org/10.1039/C0JM04112B

Cai D, Song M (2007) Preparation of fully exfoliated graphite oxide nanoplatelets in organic solvents. J Mater Chem 17:3678–3680. https://doi.org/10.1039/B705906J

Cao N, Lyu Q, Li J et al (2017) Facile synthesis of fluorinated polydopamine/chitosan/reduced graphene oxide composite aerogel for efficient oil/water separation. Chemical Engineering Journal 326:17–28. https://doi.org/10.1016/J.CEJ.2017.05.117

Chauke VP, Maity A, Chetty A (2015) High-performance towards removal of toxic hexavalent chromium from aqueous solution using graphene oxide-alpha cyclodextrin-polypyrrole nanocomposites. J Mol Liq 211:71–77. https://doi.org/10.1016/J.MOLLIQ.2015.06.044

Daemi H, Barikani M (2012) Synthesis and characterization of calcium alginate nanoparticles, sodium homopolymannuronate salt and its calcium nanoparticles. Scientia Iranica 19:2023–2028. https://doi.org/10.1016/J.SCIENT.2012.10.005

de Borja OF, Sammaraie H, Campano C et al (2022) Hexavalent chromium removal from industrial wastewater by adsorption and reduction onto cationic cellulose nanocrystals. Nanomaterials 12:4172. https://doi.org/10.3390/NANO12234172

Ferrari A, Robertson J (2000) Interpretation of Raman spectra of disordered and amorphous carbon. Phys Rev B 61:14095. https://doi.org/10.1103/PhysRevB.61.14095

Ferrari AC, Meyer JC, Scardaci V et al (2006) Raman spectrum of graphene and graphene layers. Phys Rev Lett 97:187401. https://doi.org/10.1103/PHYSREVLETT.97.187401/FIGURES/3/MEDIUM

Foo KY, Hameed BH (2010) Insights into the modeling of adsorption isotherm systems. Chemical Engineering Journal 156:2–10. https://doi.org/10.1016/J.CEJ.2009.09.013

Ge H, Ma Z (2015) Microwave preparation of triethylenetetramine modified graphene oxide/chitosan composite for adsorption of Cr(VI). Carbohydr Polym 131:280–287. https://doi.org/10.1016/J.CARBPOL.2015.06.025

Gheju M, Balcu I, Mosoarca G (2016) Removal of Cr(VI) from aqueous solutions by adsorption on MnO2. J Hazard Mater 310:270–277. https://doi.org/10.1016/j.jhazmat.2016.02.042

Gherasim CV, Bourceanu G (2013) Removal of chromium(VI) from aqueous solutions using a polyvinyl-chloride inclusion membrane: experimental study and modelling. Chem Eng J 220:24–34. https://doi.org/10.1016/J.CEJ.2013.01.058

Hashim M, Mukhopadhyay S, … JS-J of environmental, 2011 undefined (2011) Remediation technologies for heavy metal contaminated groundwater. Elsevier https://doi.org/10.1016/j.jenvman.2011.06.009

Ho YS, Ng JCY, McKay G (2011) Kinetics of pollutant sorption by biosorbents. Sep Purif Methods 29:189–232. https://doi.org/10.1081/SPM-100100009

Hozhabr Araghi S, Entezari MH, Chamsaz M (2015) Modification of mesoporous silica magnetite nanoparticles by 3-aminopropyltriethoxysilane for the removal of Cr(VI) from aqueous solution. Microporous Mesoporous Mater 218:101–111. https://doi.org/10.1016/J.MICROMESO.2015.07.008

Hsu LC, Wang SL, Lin YC et al (2010) Cr(VI) Removal on fungal biomass of *Neurospora crassa*: the importance of dissolved organic carbons derived from the biomass to Cr(VI) reduction. Environ Sci Technol 44:6202–6208. https://doi.org/10.1021/ES1017015/SUPPL_FILE/ES1017015_SI_001.PDF

Hummers WS, Offeman RE (1958) Preparation of graphitic oxide. J Am Chem Soc 80:1339–1339

Jiao C, Xiong J, Tao J et al (2016) Sodium alginate/graphene oxide aerogel with enhanced strength–toughness and its heavy metal adsorption study. Int J Biol Macromol 83:133–141. https://doi.org/10.1016/J.IJBIOMAC.2015.11.061

Karthik R, Meenakshi S (2015) Removal of Cr(VI) ions by adsorption onto sodium alginate-polyaniline nanofibers. Int J Biol Macromol 72:711–717. https://doi.org/10.1016/j.ijbiomac.2014.09.023

Kong D, Zhang F, Wang K et al (2014) Fast removal of Cr(VI) from aqueous solution using Cr(VI)-imprinted polymer particles. Ind Eng Chem Res 53:4434–4441. https://doi.org/10.1021/IE403484P

Li L, Fan L, Sun M et al (2013) Adsorbent for hydroquinone removal based on graphene oxide functionalized with magnetic cyclodextrin–chitosan. Int J Biol Macromol 58:169–175. https://doi.org/10.1016/J.IJBIOMAC.2013.03.058

Li LL, Feng XQ, Han RP et al (2017) Cr(VI) removal via anion exchange on a silver-triazolate MOF. J Hazard Mater 321:622–628. https://doi.org/10.1016/J.JHAZMAT.2016.09.029

Li X, Zhou H, Wu W et al (2015) Studies of heavy metal ion adsorption on chitosan/sulfydryl-functionalized graphene oxide composites. J Colloid Interface Sci 448:389–397. https://doi.org/10.1016/J.JCIS.2015.02.039

Liu B, Huang Y (2011) Polyethyleneimine modified eggshell membrane as a novel biosorbent for adsorption and detoxification of Cr(VI) from water. J Mater Chem 21:17413–17418. https://doi.org/10.1039/C1JM12329G

Liu C, Jin RN, Ouyang X kun, Wang YG (2017) Adsorption behavior of carboxylated cellulose nanocrystal—polyethyleneimine composite for removal of Cr(VI) ions. Appl Surf Sci 408:77–87. https://doi.org/10.1016/j.apsusc.2017.02.265

Lv X, Xue X, Jiang G et al (2014) Nanoscale zero-valent iron (nZVI) assembled on magnetic Fe3O4/graphene for chromium (VI) removal from aqueous solution. J Colloid Interface Sci 417:51–59. https://doi.org/10.1016/J.JCIS.2013.11.044

Ma HL, Zhang Y, Hu QH et al (2012) Chemical reduction and removal of Cr(VI) from acidic aqueous solution by ethylenediamine-reduced graphene oxide. J Mater Chem 22:5914–5916. https://doi.org/10.1039/C2JM00145D

Marcano DC, Kosynkin DV, Berlin JM et al (2010) Improved synthesis of graphene oxide. ACS Nano 4:4806–4814. https://doi.org/10.1021/NN1006368/ASSET/IMAGES/LARGE/NN-2010-006368_0011.JPEG

Moussavi G, Khosravi R (2010) Removal of cyanide from wastewater by adsorption onto pistachio hull wastes: parametric experiments, kinetics and equilibrium analysis. J Hazard Mater 183:724–730. https://doi.org/10.1016/J.JHAZMAT.2010.07.086

Ojembarrena FDB, ; Sánchez-Salvador JL;, Mateo S;, et al (2022) Modeling of hexavalent chromium removal with hydrophobically modified cellulose nanofibers. Polymers 14:3425. https://doi.org/10.3390/POLYM14163425

Omer AM, Khalifa RE, Hu Z et al (2019) Fabrication of tetraethylenepentamine functionalized alginate beads for adsorptive removal of Cr (VI) from aqueous solutions. Int J Biol Macromol 125:1221–1231. https://doi.org/10.1016/J.IJBIOMAC.2018.09.097

Pan C, Troyer LD, Catalano JG, Giammar DE (2016) Dynamics of chromium(VI)removal from drinking water by iron electrocoagulation. Environ Sci Technol 50:13502–13510. https://doi.org/10.1021/ACS.EST.6B03637/SUPPL_FILE/ES6B03637_SI_001.PDF

Pan C, Troyer LD, Liao P et al (2017) Effect of humic acid on the removal of chromium(VI) and the production of solids in iron electrocoagulation. Environ Sci Technol 51:6308–6318. https://doi.org/10.1021/ACS.EST.7B00371/SUPPL_FILE/ES7B00371_SI_001.PDF

Pang Y, Zeng GM, Tang L et al (2011) Cr(VI) reduction by *Pseudomonas aeruginosa* immobilized in a polyvinyl alcohol/sodium alginate matrix containing multi-walled carbon nanotubes. Bioresour Technol 102:10733–10736. https://doi.org/10.1016/J.BIORTECH.2011.08.078

Periyasamy S, Gopalakannan V, Viswanathan N (2018) Hydrothermal assisted magnetic nano-hydroxyapatite encapsulated alginate beads for efficient Cr(VI) uptake from water. J Environ Chem Eng 6:1443–1454. https://doi.org/10.1016/J.JECE.2018.01.007

Saha B, Orvig C (2010) Biosorbents for hexavalent chromium elimination from industrial and municipal effluents. Coord Chem Rev 254:2959–2972. https://doi.org/10.1016/J.CCR.2010.06.005

Saha R, Nandi R, Saha B (2011) Sources and toxicity of hexavalent chromium. 64:1782–1806. https://doi.org/10.1080/00958972.2011.583646

Samuel MS, Shah SS, Subramaniyan V et al (2018) Preparation of graphene oxide/chitosan/ferrite nanocomposite for chromium(VI) removal from aqueous solution. Int J Biol Macromol 119:540–547. https://doi.org/10.1016/J.IJBIOMAC.2018.07.052

Saslow SA, Um W, Pearce CI et al (2017) Reduction and simultaneous removal of 99Tc and Cr by Fe(OH)2(s) mineral transformation. Environ Sci Technol 51:8635–8642. https://doi.org/10.1021/ACS.EST.7B02278/SUPPL_FILE/ES7B02278_SI_001.PDF

Shakya A, Agarwal T (2019) Removal of Cr(VI) from water using pineapple peel derived biochars: adsorption potential and re-usability assessment. J Mol Liq 293. https://doi.org/10.1016/j.molliq.2019.111497

Sharma G, Naushad M, Al-Muhtaseb AH et al (2017) Fabrication and characterization of chitosan-crosslinked-poly(alginic acid) nanohydrogel for adsorptive removal of Cr(VI) metal ion from aqueous medium. Int J Biol Macromol 95:484–493. https://doi.org/10.1016/j.ijbiomac.2016.11.072

Singh DK, Kumar V, Mohan S, Hasan SH (2017) Polylysine functionalized graphene aerogel for the enhanced removal of Cr(VI) through adsorption: kinetic, isotherm, and thermodynamic modeling of the process. J Chem Eng Data 62:1732–1742. https://doi.org/10.1021/ACS.JCED.7B00188/SUPPL_FILE/JE7B00188_SI_001.PDF

Sui ZY, Cui Y, Zhu JH, Han BH (2013) Preparation of three-dimensional graphene oxide-polyethylenimine porous materials as dye and gas adsorbents. ACS Appl Mater Interfaces 5:9172–9179. https://doi.org/10.1021/AM402661T/SUPPL_FILE/AM402661T_SI_001.PDF

Tonghuan L, Xiaojiang D, Guojian D et al (2013) Adsorption of UO22+ on poly(N,N-diethylacrylamide- co-acrylic acid): effects of pH, ionic strength, initial uranyl concentration, and temperature. J Radioanal Nucl Chem 298:571–580. https://doi.org/10.1007/S10967-013-2434-X/METRICS

Vilcinskas K, Zlopasa J, Jansen KMB et al (2016) Water sorption and diffusion in (reduced) graphene oxide-alginate biopolymer nanocomposites. Macromol Mater Eng 301:1049–1063. https://doi.org/10.1002/MAME.201600154

Wang XS, Chen LF, Li FY et al (2010) Removal of Cr (VI) with wheat-residue derived black carbon: reaction mechanism and adsorption performance. J Hazard Mater 175:816–822. https://doi.org/10.1016/J.JHAZMAT.2009.10.082

Xu C, Wang X, Zhu J (2008) Graphene - metal particle nanocomposites. J Phys Chem C 112:19841–19845. https://doi.org/10.1021/JP807989B/SUPPL_FILE/JP807989B_SI_001.PDF

Yang S, Li L, Pei Z et al (2014) Adsorption kinetics, isotherms and thermodynamics of Cr(III) on graphene oxide. Colloids Surf A Physicochem Eng Asp 457:100–106. https://doi.org/10.1016/J.COLSURFA.2014.05.062

Yang Z, Xing G, Hou P, Han D (2018) Amino acid-mediated N-doped graphene aerogels and its electrochemical properties. Mater Sci Eng B 228:198–205. https://doi.org/10.1016/J.MSEB.2017.11.028

Zhang L, Luo H, Liu P et al (2016) A novel modified graphene oxide/chitosan composite used as an adsorbent for Cr(VI) in aqueous solutions. Int J Biol Macromol 87:586–596. https://doi.org/10.1016/J.IJBIOMAC.2016.03.027

Zhang Y, Yan L, Xu W et al (2014) Adsorption of Pb(II) and Hg(II) from aqueous solution using magnetic CoFe2O4-reduced graphene oxide. J Mol Liq 191:177–182. https://doi.org/10.1016/J.MOLLIQ.2013.12.015

Zhao S, Chen Z, Shen J et al (2017) Enhanced Cr(VI) removal based on reduction-coagulation-precipitation by NaBH4 combined with fly ash leachate as a catalyst. Chem Eng J 322:646–656. https://doi.org/10.1016/J.CEJ.2017.04.057

Zhou L, Liu Y, Liu S et al (2016) Investigation of the adsorption-reduction mechanisms of hexavalent chromium by ramie biochars of different pyrolytic temperatures. Bioresour Technol 218:351–359. https://doi.org/10.1016/J.BIORTECH.2016.06.102

Zhou T, Li C, Jin H et al (2017) Effective adsorption/reduction of Cr(VI) oxyanion by halloysite@polyaniline hybrid nanotubes. ACS Appl Mater Interfaces 9:6030–6043. https://doi.org/10.1021/ACSAMI.6B14079/SUPPL_FILE/AM6B14079_SI_001.PDF